ChemPubSoc Europe

DOI: 10.1002/batt.201900147

BATTERIES & SUPERCAPS Communications

Three-Sodium Ion Activity of a Hollow Spherical $Na_3V_2(PO_4)_2F_3$ Cathode: Demonstrating High Capacity and Stability

Ayan Mukherjee,[a, b] Tali Sharabani,[a, b] Ilana Perelshtein,[b] and Malachi Noked*[a, b]

$Na_3V_2(PO_4)_2F_3$ (NVPF) is a promising cathode material for sodium ion batteries, owing to its high voltage and promising cycling profile. Nevertheless, most previous reports demonstrated only approximately 100 mAh g^{-1} at limited operating voltage. Using a solvothermal synthesis route, we synthesized the NVPF cathode with a controlled architecture and spherical morphology. We used this electrode as the cathode for a sodium-ion battery and managed to intercalate/deintercalate the third Na^+ ion from the structure, demonstrating a high specific capacity (197 mAh g^{-1}). Long-term stability challenges of these electrodes under a wide potential regime are also presented here in.

Recent advances and the large-scale implementation of renewable energy systems pose a challenge to developing large energy storage technology. The most fascinating energy storage technology in mobile application are secondary batteries, of which the lithium ion batteries (LIBs) are recognized as excellent viable energy storage devices (ESD).[1–7] Due to the superior performances of LIB, and their projected utilization of batteries in electric vehicles, and due limited abundancy of lithium, alternatives to LIB technology are required for stationary large energy storage units. Hence, the search of efficient alternatives converges at sodium (Na) which is the 4th most abundance element and much lower in cost than lithium. The sodium ion batteries (SIB) demonstrates similar electrochemical intercalation behavior as Li, and considered as the most promising candidate for ESD.[8–11] However, the larger ionic radius of Na requires the development of suitable electrode material of large tunnel structure for facile intercalation/deintercalation and faster kinetics. Over the various materials, such as metal oxides,[12–14] sulfides,[15–17] phosphates,[18–20] ferrocyanides,[21,22] the NSIOCON structure shown its prominence as the most suitable candidate than others.[15,23,24] Considering the extensive research on $Na_3V_2(PO_4)_2F_3$ (NVPF) over the past few decades,[25–28] it has been observed that NVPF a promising positive electrode material for SIB which can deliver reversible capacity of 128 mAh.g^{-1} for the extraction of two Na^+ ions per formula unit via two redox plateaus at nearly 3.7 V and 4.1 V vs. Na/Na^+ with excellent stability and columbic efficiency.[8,29] In order to boost up the electrode capacity, Bianchini et al.[30] attempted to intercalate/deintercalate the third Na ion at potential window of 1.6–4.5 V (vs. Na/Na^+) which deliver specific extra capacity of 65 mAh.g^{-1}. Very Recently, Yan et. al.[31] demonstrated the feasibility to increase the charging voltage up to 4.8 vs Na/Na^+ and discharging down to 1 V vs Na/Na^+ and observed a structural phase transformation in NVPF from orthorhombic to tetragonal. They observed a sodium-driven structural/charge compensation mechanism along with a new phase which remains disordered upon cycling with varying average vanadium oxidation state from 3 to 4.5. These two previous reports, relied on solid state synthesis of NVPF, with limited control over architecture and morphology of the active material. Additionally, these two great works, focused on initial cycling with reported electrochemical responses in half cells of up to 3[30] or 25 cycle.[31] Using novel synthesis pathway, we demonstrate herein an accurate control over NVPF morphology and prepared micro hollow spheres (MHS) which crystalizes in orthorhombic structure. This unique morphology enabled a significant improvement in electrode capacity, in the voltage window of 1 V to 4.8 V (vs. Na/Na^+) in high (80 mA.g^{-1}) and low (10 mA.g^{-1}) current rates. Additionally, we visit here in for the 1st time the long-term effect of 3 Na + intercalation/deintercalation under the wide operating voltage range (1 V to 4.8 V), on the stability of the cathode. Our report demonstrates highest reported capacity of NVPF, with proposed strategies for stabilizing this electrode for long term cycling stability.

NVPF micro-hollow spheres (MHS) was prepared by a facile solvothermal route using ammonium metavanadate, sodium fluoride and sodium phosphate as metal precursors, tetraethylene glycol and water as solvents at 200 °C. The details of electrochemical measurements and physical characterization (x-ray diffractometer (XRD), High resolution scanning electron microscope (HRSEM), High resolution transmission electron microscope (HRTEM)and Inductively coupled plasma mass spectrometry (ICP-AES)) are explained in detail in the electronic supporting information (ESI).

The XRD pattern of the sample presented in Figure 1 (a) corresponds to a phase pure NVPF having Pnnm space group.[32] Inset shows the crystal structure of NVPF which visualize that the open 3D framework with large channels should facilitate the sodium ions diffusion easily. The exact stoichiometry is further confirmed from the Na/V ratio, obtained from ICP-AES, which is 1.501. The morphology of the

[a] Dr. A. Mukherjee, T. Sharabani, Dr. M. Noked
Department of Chemistry
Bar Ilan University
Ramat Gan, Israel
E-mail: malachi.noked@biu.ac.il
[b] Dr. A. Mukherjee, T. Sharabani, Dr. I. Perelshtein, Dr. M. Noked
Bar-Ilan Institute of Nanotechnology and Advanced Materials,
Ramat Gan, Israel

Supporting information for this article is available on the WWW under https://doi.org/10.1002/batt.201900147

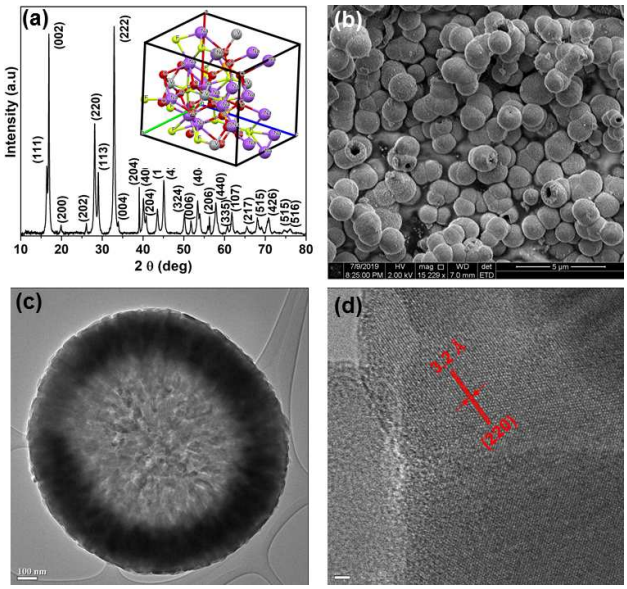

Figure 1. a) XRD pattern and the inset shows the crystal structure; b) SEM, c) TEM, and d) HRTEM images of NVPF.

NVPF is characterized by SEM and TEM as shown in Figure 1 (b) and (c) respectively. The NVPF exhibit micro-hollow spherical structure of 2 μm size which is assembled by nanoplates as shown in Figure S1. The typical HRTEM image shown in Figure 1 (d) further confirm the crystalline nature and phase purity of NVPF. The lattice spacing (*d*) of 3.2 Å matches with (220) plane of NVPF.

Voltage profile within the often-used potential regime for charge\discharge (2 Na^+ insertion\extraction) is presented in Figure2 (a), it is clear that our material is state of the art NVPF with high capacity and high kinetics (Figure 2 (b)). The

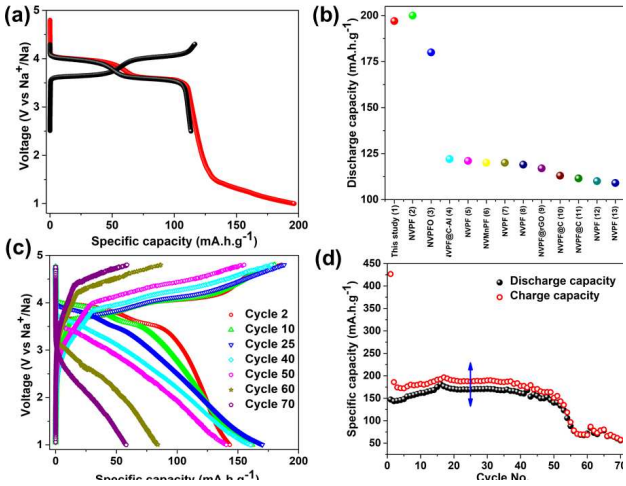

Figure 2. a) Charge/discharge profile of NVPF at 10 mA/g. b) Specific capacity comparison of our NVPF with state-of-the-art NVPF; numbers in parentheses refer to references: 1) this study, 2) Ref. [31], 3) Ref. [30], 4) Ref. [36], 5) Ref. [37] 6)Ref. [38], 7) Ref. [31], 8) Ref. [39], 9) Ref. [40], 10) Ref. [41], 11) Ref. [41], 12) Ref. [42], 13) Ref. [43]. c) Charge/discharge profile. d) Cycling profile of NVPF-HP (blue line indicates the limit of measurement of previous study) at 80 $mA.g^{-1}$.

impressive cycling stability (98%) of up to 500 cycles (Figure S2), also support the high quality of our NVPF. To boost the capacity of our material even farther, we expanded the potential widow to 1 V–4.8 V (vs. Na/Na^+), designated as NVPF-HP shows the 1st cycle of the NVPF-HP, which mirrors the insertion of more than 2 Na from NVPF structure from the appearance of three distinct discharge plateaus at 4.0 V, 3.6 V and 1.2 V and deliver discharge capacity of 197 $mA.h.g^{-1}$ at 10 $mA.g^{-1}$ (Supporting Information, Figure S3), similar to recent report by Tarascon et al..[31] Figure 2 (b) represent a comparison between our NVPF capacity, and previous reports. We attribute the high capacity to the distinct morphology of our cathode, which renders the active material fully accessible for sodium ion diffusion, and to the well control orthorhombic crystal structure obtained through our synthesis. Previous reports attempted to boost the capacity of NVPF has shown maximum cycles number of 25, therefore we can't comment on the longevity of previously synthesized NVPF.

We explore here for the first time the effect of prolonged cycling on the crystal structure of NVPF and its performances. In order to do so, we cycled the NVPF in relatively high currents (80 $mA.g^{-1}$), hence the obtained capacity is lower than in the slow rates. Figure 2 (c) and (d) respectively shows the galvanostatic charge/discharge profile and long cycling of NVPF-HP cycled at current density of 80 $mA.g^{-1}$. The NVPF-HP maintains high discharge capacity of ~160 $mA.h.g^{-1}$ up to 50 cycles, but suddenly loses the capacity and kinetics quickly and delivers discharge capacity of only 84 $mA.h.g^{-1}$ and 58 $mA.h.g^{-1}$ in 60th and 70th cycle respectively. It is also observed from Figure S4 (Supporting Information) that the CE is nearly stable at 90% up to 50 cycles which is much higher than previous report in the measured potential regime[31] but degrades consistently into subsequent cycles and remains only 40% in 70th cycle. The chemical degradation mechanism might be accounted for the instability of the NVPF in the measured potential window (1 V–4.8 V (vs. Na/Na^+)),due to phase transformation as reported by Tarascon .[31] Additionally, the high potential during charging is beyond the anodic stability of the alkyl carbonate solution, what induce the formation of cathode electrolyte interphase (CEI). Furthermore, solvent co-intercalation and active material dissolution also plays crucial role in the degradation pathway.[33] These processes creates favorable condition for side reaction to occur,[34,35] which eventually degrade the electrode material significantly. Hence, charging the NVPF-HP up to 4.8 V (vs. Na/Na^+) and discharging down to 1 V (vs. Na/Na^+) to extract and insert the third Na^+ ion from the NVPF structure accounted for the quick degradation and failure of the overall cell. To further understand these instabilities, the morphology of the NVPF-HP electrode before cycling, post-mortem after 70 cycles at 80 $mA.g^{-1}$ and 40 cycles at 10 $mA.g^{-1}$is shown in Figure 3. It is observed from Figure 3 (a) and (b) that NVPF-HP retains its MHS morphology after forming the final electrode for cycling and distributed uniformly throughout the electrode. After cycling for 70 cycles at 80 $mA.g^{-1}$, as shown in Figure 3 (c), a thin layer is formed which covers throughout the surface of the MHS. Figure 3 (d) confirms the ultimate degradation of the NVPF-HP through the

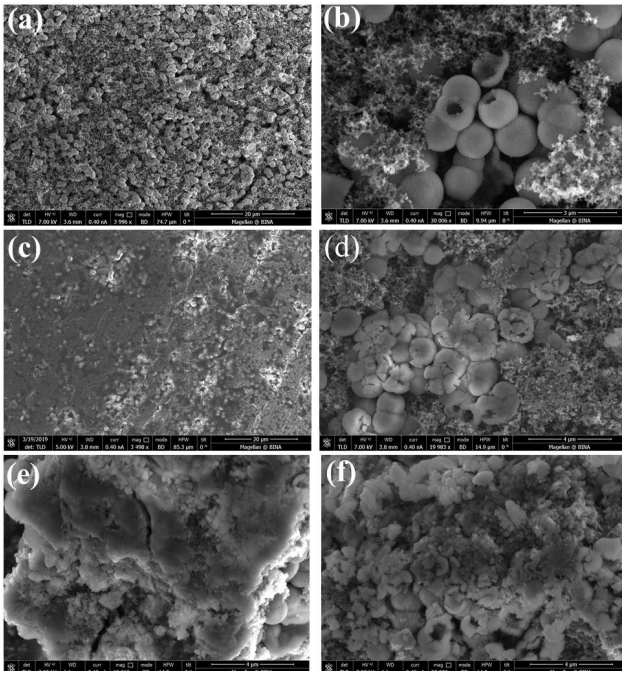

Figure 3. HRSEM images of a, b) bare NVPF slurry, c, d) NVPF-HP cycled after 70 cycles at 80 mA.g^{-1} and e, f) NVPF-HP cycled after 40 cycles at 10 mA.g^{-1}.

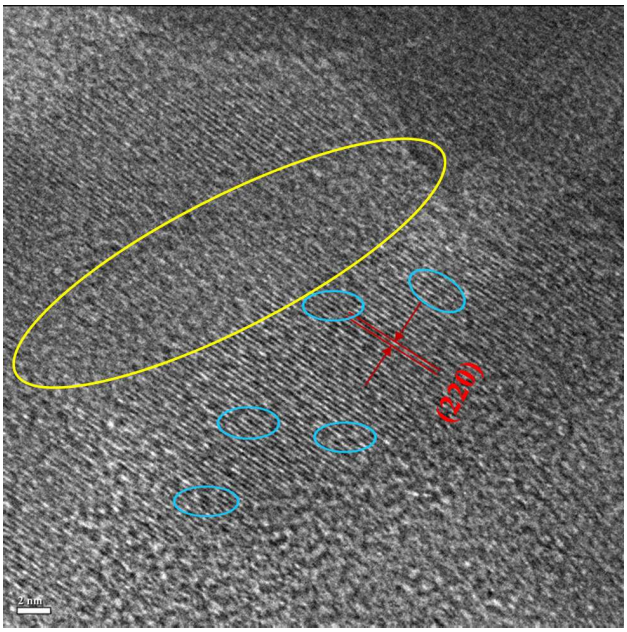

Figure 4. HRTEM image of NVPF-HP cycled at 80 mA.g^{-1} after 70 cycles.

appearance of micro cracks in the MHS and eventually collapse of the whole structure as observed from the disappearance of charge/discharge plateaus (Figure 2 (d)). Figure 3 (e) and (f) shows that the degradation is more pronounced at lower current rate where the MHS suffers significant cleavage even after just 40 cycles. Further, the degradation of NVPF-HP cycled at 80 mA.g^{-1} for 70 cycles is visualized more distinctly in Figure S5(supporting Information) from different magnification of HRSEM images and can be observed that in the measured potential window (1 V–4.8 V (vs. Na/Na$^+$)), chemical degradation pave a significant impact for the degradation of the NVPF-HP and not suitable for practical application. The structural degradation can further be explicitly understood from the post-mortem XRD and HRTEM analysis.

The post-mortem XRD study of NVPF-HP cycled at 80 mA.g^{-1} and NVPF electrode before cycling is shown in Figure S6 (supporting Information), clearly reflects the significant loss in the crystallinity through the decrease in the intensity of the (002), (220), (113) and (222) diffraction planes. The most preferred oriented plane in NVPF(222) exhibit a shifting towards lower angle shown in the Figure S7 (supporting Information) signifying the increase in *d* spacing due to Na$^+$ ion intercalation/deintercalation. The TEM images (Figure S8 (supporting Information)) shows that the MHS morphology is completely destroyed after 70th cycle whereas the HRTEM image shown in Figure 4 clearly visualizes that the NVPF-HP losses the crystallinity (shown by yellow oval) and more precisely, the *d* spacing of (220) plane increases from 3.20 Å to 3.34 Å with distinct distortion in parallel lattice planes (shown by blue circles).Such structural and morphological degradation explicitly reflects in the electrochemical performance through the failure of the cell in the measured potential window. Further, in order to compare the performance we have cycled few NVPF-NP cathode in the potential widow of 2.5 V to 4.3 V (vs. Na/Na$^+$) at 80 mA.g^{-1}, shown in Figure S9 (supporting Information). It is observed that after 10th cycle (Figure S9a (supporting Information)) and 25th cycle (Figure S9b (supporting Information)), NVPF-HP exhibit higher specific capacity than NVPF-NP with distinct plateaus, demonstrating pronounced Na$^+$ ion intercalation/deintercalation. However, within 50 cycles (Figure S9c (supporting Information)), NVPF-HP lost its plateaus and after 70 cycles (Figure S9d (supporting Information)) lost the specific capacity significantly whereas, NVPF-NP retain its distinct plateaus and maintain specific capacity with negligible losses.

In summary, hierarchical micro hollow spheres of NVPF (average size ~2 μm) composed of nanoplates has been prepared by a facile solvothermal route. The phase purity, crystallinity and morphology are established through XRD, HRTEM and HRSEM studies respectively. As a cathode for SIB, NVPF showed pronounced specific capacity of 197 mA.h.g^{-1} at 10 mA.g^{-1} and 160 mA.h.g^{-1} at 80 mA.g^{-1} through the intercalation/deintercalation of third Na$^+$ ion from NVPF and maintains the capacity up to 25 cycles. However, structural and morphological instabilities in the measured potential window (1 V–4.8 V (vs Na/Na$^+$)) accounted for poor cycling stability, even after 40 cycles, due to chemical degradation mechanism of electrolyte on the cathode and due to the loss of crystallinity of the NVPF. Our studies indicate that significant capacity enhancement is possible with NVPF, however instabilities must be addressed before the large voltage window can be practically realized. We propose future strategies that are based on coating or doping of the active material to address these degradation pathways.

Conflict of Interest

The authors declare no conflict of interest.

Keywords: high-voltage cathodes · cathode materials · $Na_3V_2(PO_4)_2F_3$ · intercalation · sodium-ion batteries

[1] M. N. E. Evenstein, Rosy, S. Haber, H. Sclar, L. Houben, K. Leung, M. Leskes, *Energy Storage Mater.* **2018**, 1–9.
[2] K. N. Wood, M. Noked, N. P. Dasgupta, *ACS Energy Lett.* **2017**, *2*, 664–672.
[3] D. Sharon, D. Hirsberg, M. Salama, M. Afri, A. A. Frimer, M. Noked, W. Kwak, Y. K. Sun, D. Aurbach, *ACS Appl. Mater. Interfaces* **2016**, *8*, 5300–5307.
[4] A. C. Kozen, C. F. Lin, A. J. Pearse, M. A. Schroeder, X. Han, L. Hu, S. B. Lee, G. W. Rubloff, M. Noked, *ACS Nano* **2015**, *9*, 5884–5892.
[5] A. C. Kozen, A. J. Pearse, C. F. Lin, M. A. Schroeder, M. Noked, S. B. Lee, G. W. Rubloff, *J. Phys. Chem. C* **2014**, *118*, 27749–27753.
[6] Z. Yang, J. Zhang, M. C. W. Kintner-Meyer, X. Lu, D. Choi, J. P. Lemmon, J. Liu, *Chem. Rev.* **2011**, *111*, 3577–3613.
[7] J. B. Goodenough, Y. Kim, *Chem. Mater.* **2010**, *22*, 587–603.
[8] H. Pan, Y. S. Hu, L. Chen, *Energy Environ. Sci.* **2013**, *6*, 2338–2360.
[9] M. D. Slater, D. Kim, E. Lee, C. S. Johnson, *Adv. Funct. Mater.* **2013**, *23*, 947–958.
[10] S. P. Ong, V. L. Chevrier, G. Hautier, A. Jain, C. Moore, S. Kim, X. Ma, G. Ceder, *Energy Environ. Sci.* **2011**, *4*, 3680–3688.
[11] N. Yabuuchi, K. Kubota, M. Dahbi, S. Komaba, *Chem. Rev.* **2014**, *114*, 11636–11682.
[12] Y. Wang, X. Yu, S. Xu, J. Bai, R. Xiao, Y. S. Hu, H. Li, X. Q. Yang, L. Chen, X. Huang, *Nat. Commun.* **2013**, *4*, 2365–2371.
[13] D. Yuan, X. Liang, L. Wu, Y. Cao, X. Ai, J. Feng, H. Yang, *Adv. Mater.* **2014**, *26*, 6301–6306.
[14] J. Xu, C. Ma, M. Balasubramanian, Y. S. Meng, *Chem. Commun.* **2014**, *50*, 12564–12567.
[15] Y. Fang, L. Xiao, J. Qian, X. Ai, H. Yang, Y. Cao, *Nano Lett.* **2014**, *14*, 3539–3543.
[16] Z. Jian, L. Zhao, H. Pan, Y. S. Hu, H. Li, W. Chen, L. Chen, *Electrochem. Commun.* **2012**, *14*, 86–89.
[17] S. M. Oh, S. T. Myung, J. Hassoun, B. Scrosati, Y. K. Sun, *Electrochem. Commun.* **2012**, *22*, 149–152.
[18] X. Zhong, Z. Yang, Y. Jiang, W. Li, L. Gu, Y. Yu, *ACS Appl. Mater. Interfaces* **2016**, *8*, 32360–32365.
[19] S. Hu, L. Scudiero, S. Ha, *Electrochim. Acta* **2012**, *83*, 354–358.
[20] A. Serov, C. Kwak, *Appl. Catal. B* **2010**, *97*, 1–12.
[21] C. D. Wessells, S. V. Peddada, R. A. Huggins, Y. Cui, *Nano Lett.* **2011**, *11*, 5421–5425.
[22] L. Wang, Y. Lu, J. Liu, M. Xu, J. Cheng, D. Zhang, J. B. Goodenough, *Angew. Chem. Int. Ed.* **2013**, *52*, 1964–1967.
[23] K. Saravanan, C. W. Mason, A. Rudola, K. H. Wong, P. Balaya, *Adv. Energy Mater.* **2013**, *3*, 444–450.
[24] Z. Zhou, D. Chen, H. Yang, X. Lu, Y.-S. Hu, W. Chen, Z. Jian, W. Han, L. Chen, J. Li, *Adv. Energy Mater.* **2013**, *3*, 156–160.
[25] W. Song, X. Ji, J. Chen, Z. Wu, Y. Zhu, K. Ye, H. Hou, M. Jing, C. E. Banks, *Phys. Chem. Chem. Phys.* **2015**, *17*, 159–165.
[26] H. Li, Y. Bai, F. Wu, Q. Ni, C. Wu, *ACS Appl. Mater. Interfaces* **2016**, *8*, 27779–27787.
[27] T. Broux, T. Bamine, F. Fauth, L. Simonelli, W. Olszewski, C. Marini, M. Ménétrier, D. Carlier, C. Masquelier, L. Croguennec, *Chem. Mater.* **2016**, *28*, 7683–7692.
[28] W. Liu, H. Yi, Q. Zheng, X. Li, H. Zhang, *J. Mater. Chem. A* **2017**, *5*, 10928–10935.
[29] R. K. B. Gover, A. Bryan, P. Burns, J. Barker, *Solid State Ionics* **2006**, *177*, 1495–1500.
[30] M. Bianchini, P. Xiao, Y. Wang, G. Ceder, *Adv. Energy Mater.* **2017**, *7*, 1–9.
[31] G. Yan, S. Mariyappan, G. Rousse, Q. Jacquet, M. Deschamps, R. David, B. Mirvaux, J. W. Freeland, J. M. Tarascon, *Nat. Commun.* **2019**, *10*, 585.
[32] Y. Zhang, S. Guo, H. Xu, *J. Mater. Chem. A* **2018**, *6*, 4525–4534.
[33] D. E. Demirocak, B. Bhushan, *J. Power Sources* **2015**, *280*, 256–262.
[34] M. Broussely, P. Biensan, F. Bonhomme, P. Blanchard, S. Herreyre, K. Nechev, R. J. Staniewicz, *J. Power Sources* **2005**, *146*, 90–96.
[35] R. E. W. Pankay Arora, M. D. Pankaj Arora, *J. Electrochem. Soc.* **1998**, *145*, 3647–3667.
[36] D. Ma, L. L. Zhang, T. Li, C. Liu, G. Liang, Y. X. Zhou, X. L. Yang, *Electrochim. Acta* **2018**, *283*, 1441–1449.
[37] Y. Qi, L. Mu, J. Zhao, Y. S. Hu, H. Liu, S. Dai, *J. Mater. Chem. A* **2016**, *4*, 7178–7184.
[38] Y. Zhang, S. Guo, H. Xu, *J. Mater. Chem. A* **2018**, *6*, 4525–4534.
[39] X. Ji, M. Jing, J. Chen, H. Hou, Q. Lan, Z. Wu, W. Song, C. Pan, Y. Zhu, Y. Yang, *Electrochim. Acta* **2014**, *146*, 142–150.
[40] Y. Cai, X. Cao, Z. Luo, G. Fang, F. Liu, J. Zhou, A. Pan, S. Liang, *Adv. Sci.* **2018**, *5*, DOI 10.1002/advs.201800680.
[41] Q. Liu, D. Wang, X. Yang, N. Chen, C. Wang, X. Bie, Y. Wei, G. Chen, F. Du, *J. Mater. Chem. A* **2015**, *3*, 21478–21485.
[42] X. J. Weixin Song, Xiaoyu Cao, Zhengping Wu, Jun Chen, Yirong Zhu, Hongshuai Hou, Qing Lan, *Langmuir* **2014**, *30*, 12438–12446.
[43] N. V. Kosova, D. O. Rezepova, S. A. Petrov, A. B. Slobodyuk, *J. Electrochem. Soc.* **2017**, *164*, A6192–A6200.

Manuscript received: October 6, 2019
Accepted manuscript online: October 19, 2019
Version of record online: November 7, 2019